JOURNAL OF SOLID STATE CHEMISTRY 118, 43–52 (1995)

Lattice Vibration Spectra

LXXXIV. Lattice Dynamics of Spinel-Type $CoCr_2S_4$, $ZnCr_2S_4$, $ZnCr_2Se_4$, $CdCr_2Se_4$, and $HgCr_2Se_4$[1]

J. Zwinscher and H. D. Lutz[2]

Universität Siegen, Anorganische Chemie I, D-57068 Siegen, Germany

Received September 23, 1994; in revised form January 9, 1995; accepted January 10, 1995

DEDICATED TO PROFESSOR DIRK REINEN ON THE OCCASION OF HIS 65TH BIRTHDAY

Lattice dynamical calculations of ACr_2X_4 spinel-type chromium chalcides $CoCr_2S_4$, $ZnCr_2S_4$, ($CdCr_2S_4$), $ZnCr_2Se_4$, $CdCr_2Se_4$, and $HgCr_2Se_4$ were performed using short-range (SRM), rigid-ion (RIM) and polarizable-ion models (PIM) with structure data, symmetry coordinates, IR and Raman frequencies, permittivities, and the masses of the atoms involved as input parameters. The mean deviations between calculated and observed phonon energies are in the range 1–5 cm^{-1} (PIM). The results obtained are discussed with respect to the change in the short-range force constants (A–X, Cr–X, Cr–Cr, and X–X valence and repulsive forces), dynamical effective ionic charges, eigenvectors, and potential energy distributions within the compounds studied, the potential models used, and the reliability of the structural parameters available, respectively. Thus, the force constants due to the tetrahedral A–X bonds are in the order $CoCr_2S_4 < ACr_2S_4 < ACr_2Se_4$ (A = Zn, Cd, Hg). Those due to the octahedral Cr–X bonds increase on going from SRM to PIM calculations, indicating (in addition to the respective effective charges) the more ionic nature of this bond compared to that of the A–X bonds.

INTRODUCTION

One of the few ways of determining the strength of individual bonds in solids is force constant calculations. Thus, recently we reported on lattice dynamical calculations of the spinel-type sulfides $MnCr_2S_4$, $FeCr_2S_4$, and $CdCr_2S_4$ using short-range (SRM), rigid-ion (RIM), and polarizable-ion (PIM) model force fields for each (1). The main results obtained are that (i) there are unexpectedly strong bonding interactions between the octahedrally coordinated metal ions (see Fig. 1), (ii) the bonding of the tetrahedral AS_4 units (A, bivalent metal) is mainly covalent, (iii) the sequence of the stretching (valence) force constants K_1 (AS_4 tetrahedron) and K_2 (CrS_6 octahedron) are $K_2 > K_1$ (in contrast to older force constant calculations (2–4)), and (iv) the total symmetric Raman-allowed AS_4 breathing modes (species A_{1g}) exhibit larger contributions of S–S repulsive force constants than those of the A–S valence force constants (contrary to conclusions drawn from Raman single crystal studies (5)). The validity of these conclusions, which are supported by very recent central and angular force model calculations of Gupta *et al.* (6–8), for spinel-type oxides and chlorides was proved in Ref. (9, 10).

In this paper, we extended our calculations on the spinel-type selenides $ZnCr_2Se_4$, $CdCr_2Se_4$, and $HgCr_2Se_4$, and the sulfides $ZnCr_2S_4$ and $CoCr_2S_4$, for which high-level lattice dynamical calculations are not available thus far. More crude force constant calculations of the title compounds or those using the central and angular force model, which is restricted to the ideal spinel structure with the structural parameter $u = 0.250$, are given in Ref. (3, 4, 6, 8, 11). IR and Raman spectroscopic data of the chalcogenides under investigation have been reported in Ref. (5, 12–19).

STRUCTURE DATA, SYMMETRY COORDINATES, PHONON ENERGIES, AND CALCULATION PROCEDURE

Normal spinel-type compounds crystallize in the space group $Fd\bar{3}m$ with two formula units in the *primitive* rhombohedral unit cell. Part of the structure is shown in Fig. 1. The unit-cell dimensions a (pm) and structural parameters u used for the presented calculations are 992.4 pm (20, 21) and 0.258 (22) ($CoCr_2S_4$), 998.6 pm and 0.259 (21) ($ZnCr_2S_4$), 1049.78 pm (23) 0.260 (24) ($ZnCr_2Se_4$), 1074.1 pm (23) and 0.2642 (25) ($CdCr_2Se_4$), and 1074.0 pm and 0.264 (26) ($HgCr_2Se_4$), respectively. The interatomic distances (pm) and angles (°) derived from the above values are given in Table 1. For the symmetry coordinates of the zone-center lattice modes ($|\vec{k}| = 0$) of spinel-type compounds, $\Gamma = A_{1g} + E_g + F_{1g} + 3F_{2g} + 2A_u + 2E_u +$

[1] Part LXXXIII, H. D. Lutz, K. Beckenkamp, and St. Peter, *Spectrochim. Acta*, in press.

[2] To whom correspondence should be addressed.

0022-4596/95 $12.00

TABLE 1
Short-Range Force Constants and Interatomic Distances and Angles

Internal coordinate	Force constant	No.[a]	Interatomic distances (pm) and angles(°)		
			$CoCr_2S_4$	$CdCr_2Se_4$	$HgCr_2Se_4$
A–X	K_1	8	228.6	258.6	258.6
Cr–X	K_2	24	240.4	254.4	254.4
Cr–Cr	F_1	12	350.9	379.8	379.7
X–A–X	H_1	12	109.5	109.5	109.5
X–Cr–X	H_2	48	93.8	97.0	97.0
			86.2	83.0	83.0
X–X (1)	F_2	12	373.3	422.3	422.2
X–X (2)	F_3	12	328.4	337.2	337.2
X–X (3)	F_4	24	351.2	380.9	380.9

Note. For the lattice constants and structural parameters u, see text; for values $ZnCr_2S_4$ and $ZnCr_2Se_4$ see Ref. (27, 28).

[a] Number of internal coordinates, those of k (AX–CrX) are 24.

$4F_{1u} + 2F_{2u}$, see Ref. (1). The phonon energies (cm^{-1}) used for computing the model parameters are given in Table 2.

The potential models (SRM, PIM) and calculation procedures used are described elsewhere (1). The dynamical matrix **D** is given by $\mathbf{D} = \mathbf{M}(\mathbf{F}^N + \mathbf{F}^C + \mathbf{F}^I + \mathbf{F}^M)\mathbf{M}$, where **M** is a diagonal matrix specifying $m^{-1/2}$ of the masses, m, involved. $\mathbf{F}^N$ is a matrix representing the non-Coulombic short-range interactions (short-range force constants), $\mathbf{F}^C$ is a diagonal matrix containing the effective dynamical charges, $\mathbf{F}^I$ is an additional Coulomb interaction matrix due to induced dipoles, and $\mathbf{F}^M$ is the macroscopic field matrix describing the TO/LO splittings of the phonons. The number and nature of the short-range force constants used for the dynamical matrix were transferred from other spinel-type compounds (1, 9, 10). The input parameters are the unit-cell dimensions a, the structural parameters u, the masses of the atoms involved, the symmetry coordinates q_n, the phonon energies FRQ, and the permittivities ε_∞. The force constants (K_i, F_i, H_i, and k_i; see Fig. 1 and Table 1), the effective dynamical charges z_k, and the polarizabilities α_k are treated as variable parameters to give the best fit of the experimental data. In doing so, special importance was given to reproducing the experimental TO/LO splittings.

RESULTS

The phonon energies (FRC), short-range force constants, effective dynamical charges, polarizabilities, eigenvectors of the phonon modes, and potential energy distributions (PED) determined are given in Tables 2–8. The vibrational modes of the zone-center phonons are shown in Figs. 2 and 3. The energies of the silent zone-center phonons and the respective vibrational modes are included. The missing Raman modes of species F_{2g} of $CoCr_2S_4$ and $ZnCr_2Se_4$ (27) have been calculated to be 111 and 242 cm^{-1}, respectively.

In order to prove the reliability of the various potential models used, the force constants of $CdCr_2Se_4$ were computed without the use of the wavenumber of the F_{2g} (1) mode (28). Deviation of the wavenumber predicted for this mode from the observed one (225 cm^{-1}) was 5, 13, and 10 cm^{-1} for the PIM, RIM, and SRM calculation, respectively. This reveals that the PIM model is the most dependable.

From model calculations using different structure data of $CdCr_2Se_4$ reported in the literature, e.g., a = 1072.1 pm and u = 0.258 (2), and a = 1073.1 pm, and u = 0.264 (25), we find that the short-range force constants K_1 and K_2 are insensitive to changes in the distances (28). However, incorrect bond lengths strongly affect the effective dynamical charges and the polarizabilities, and to a lesser extent the repulsion force constants F_2–F_4.

The short-range force constants obtained for the spinel-type chromium selenides differ from those of the respective sulfides (1) (and oxides (9)) in such a manner that (i) in the selenides the Cr–Cr (F_1) and the X–X (F_2–F_4) repulsive forces are negligible or at least considerably smaller and (ii) the A–X (K_1) valence force constants (AX_4 tetrahedron) are partly larger than those of the CrX_6 octahedra (Cr–X, K_2) with K_1 significantly increasing from $ZnCr_2Se_4$ to $HgCr_2Se_4$, viz. 0.82, 0.94, and 1.03 N cm^{-1} (PIM). The bending (H_i) and interaction force constants (k) are <0.1 N cm^{-1}. The short-range force constants of $CoCr_2S_4$ resemble those of ACr_2S_4 (A = Mn, Fe) (1); those

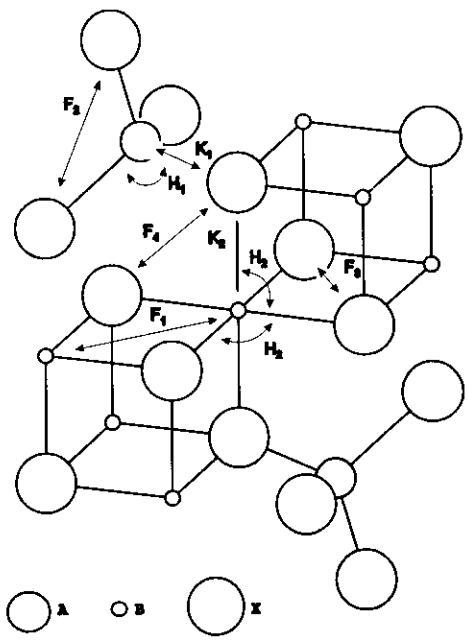

FIG. 1. Sketch of the spinel structure AB_2X_4 with the short-range force constants K_i, F_i, and H_i.

TABLE 2

Observed (FRQ) and Calculated (FRC) Phonon Frequencies (cm^{-1}) of $CoCr_2S_4$, $CdCr_2Se_4$, and $HgCr_2Se_4$

	$CoCr_2S_4$				$CdCr_2Se_4$			$HgCr_2Se_4$		
		FRC				FRC			FRC	
Species	FRQ (5, 18, 19)	SRM	RIM	PIM	FRQ (2, 12, 13, 18)	SRM	PIM	FRQ (13, 16, 18)	SRM	PIM
A_{1g}	380	382	383	378	237–240	234	234	237	231	231
E_g	252–254	251	249	256	154–157	151	154	157	153	154
F_{2g} (1)	361	362	362	361	225–226	228	228	210	219	219
F_{2g} (2)	294	290	291	295	169–171	169	169	168	167	167
F_{2g} (3)	—	113	110	111	84–85	84	85	65	67	68
F_{1u} (1) TO	388	392	395	390	288	289	288	286	292	287
F_{1u} (1) LO	400		395	400	293		293	291		295
F_{1u} (2) TO	330	330	330	330	267–264	266	267	268–270	263	264
F_{1u} (2) LO	346		345	348	281		280	282		277
F_{1u} (3) TO	265	259	262	267	186	184	186	169	166	168
F_{1u} (3) LO	266		263	268	188		187	172	65	169
F_{1u} (4) TO	124	130	128	128	75	80	77	55–58		59
F_{1u} (4) LO	126		129	130	77		78	58–60		60
A_{2u} (1)		447	456	497		285	312		295	305
A_{2u} (2)		345	340	346		190	188		176	174
E_u (1)		378	380	390		252	252		259	255
E_u (2)		248	247	240		116	90		96	73
F_{1g}		252	254	260		141	142		145	144
F_{2u} (1)		340	344	343		255	245		257	249
F_{2u} (2)		153	151	131		77	53		62	45
$\Delta\omega$		3.4	3.1	2.0		2.4	1.3		5.5	3.8

Note. SRM, RIM, and PIM, short-range, rigid-ion, and polarizable-ion models, respectively; figure of merit $\Delta\omega = \sqrt{(1/N)\sum_{i=1}^{N}(\mathrm{FRQ}(i) - \mathrm{FRC}(i))^2}$. For values for $ZnCr_2S_4$ and $ZnCr_2Se_4$ see Ref. (27, 28).

TABLE 3

Short-Range Force Constants (N cm^{-1}), Effective Dynamical Charges (e), and Electronic Polarizabilities (10^6 pm^3) of $CoCr_2S_4$, $CdCr_2Se_4$, and $HgCr_2Se_4$

Internal coordinate	Force constant	$CoCr_2S_4$			$CdCr_2Se_4$		$HgCr_2Se_4$	
		SRM	RIM	PIM	SRM	PIM	SRM	PIM
A–X	K_1	0.50	0.49	0.51	0.95	0.94	0.99	1.03
Cr–X	K_2	0.74	0.78	0.90	0.72	0.88	0.78	0.91
Cr–Cr	F_1	0.45	0.47	0.61	0.0	0.05	0.00	0.01
AX–CrX	k	0.01	0.00	0.00	0.01	0.00	0.00	0.00
X–A–X	H_1	0.00	0.00	0.00	0.00	0.00	0.00	0.00
X–Cr–X	H_2	0.03	0.03	0.01	0.03	0.01	0.01	0.01
X–X (1)	F_2	0.17	0.16	0.13	0.07	0.09	0.06	0.06
X–X (2)	F_3	0.16	0.16	0.18	0.14	0.11	0.15	0.11
X–X (3)	F_4	0.17	0.17	0.17	0.04	0.03	0.05	0.03
z_A			0.00	0.00		0.10		0.10
z_{Cr}			0.62	0.60		0.71		0.69
z_X			−0.31	−0.30		−0.38		−0.37
$z_X^{\dagger}$			−0.40	−0.40		−0.41		−0.39
α_A				2.6		2.1		2.3
α_{Cr}				0.8		0.11		0.10
α_X				3.50		5.88		6.00
ε_∞				9.1		9.7		11.2
$\varepsilon_\infty^{\dagger}$				8.3		8.9		10.9

Note. $z_X^{\dagger}$, Szigeti charge obtained from the TO/LO splittings; $\varepsilon_\infty^{\dagger}$, high-frequency dielectric constant determined by oscillator-fit calculations (18); for further explanations see Table 2. For values for $ZnCr_2S_4$ and $ZnCr_2Se_4$ see Ref. (27, 18).

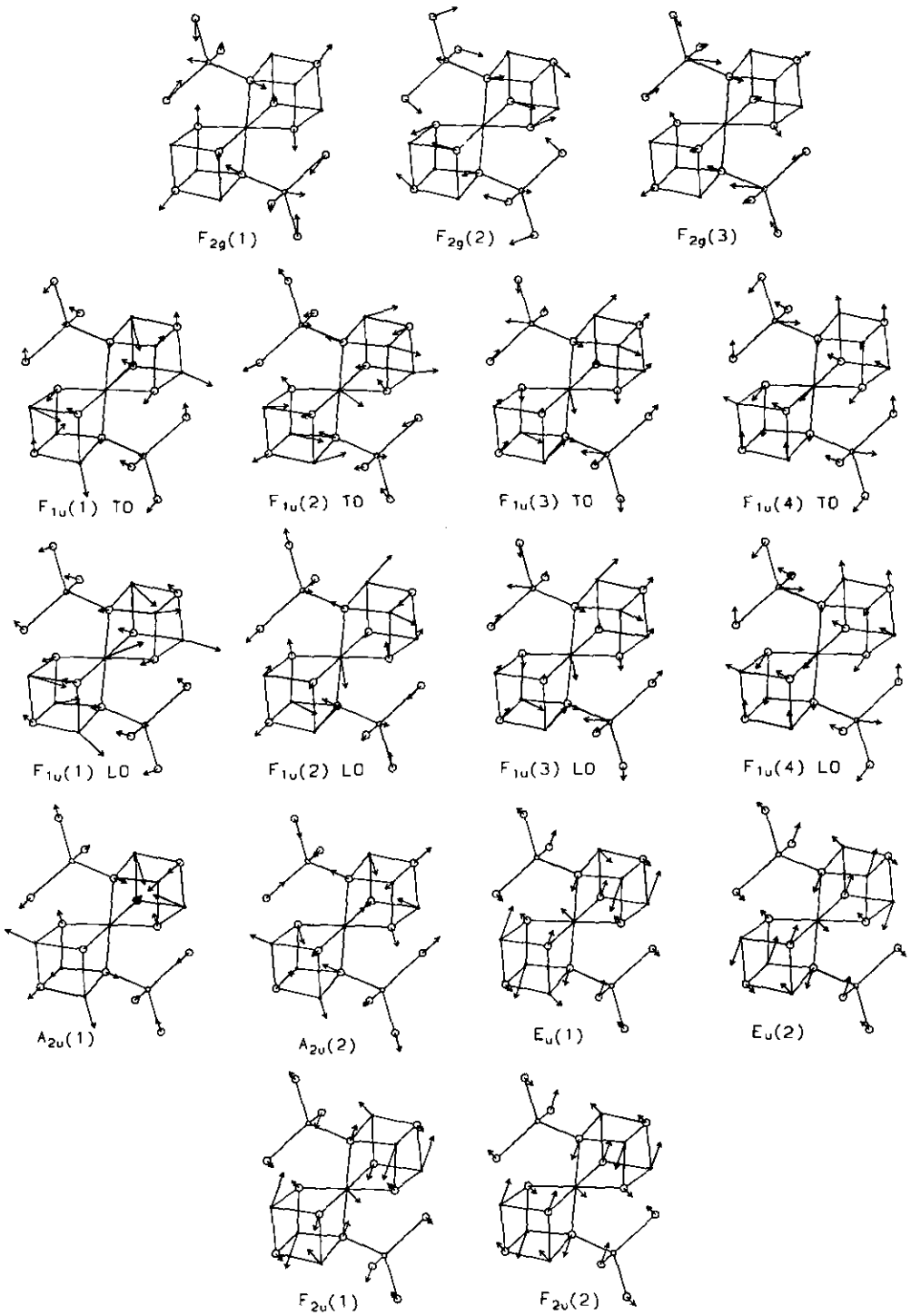

FIG. 2. Vibrational modes of the zone-center phonons of $CdCr_2Se_4$ obtained by polarizable ion model calculations; for those of the other compounds under study see Ref. (28). The vibrational modes of the phonons of species A_{1g}, E_g, and F_{1g} are restricted to the respective symmetry coordinates (1).

of $ZnCr_2S_4$ and $CdCr_2S_4$ are intermediate between the former and those of the chromium selenides, especially with respect to K_1 (see Table 3).

The effective dynamical charges of spinel-type chromium selenides are somewhat smaller than those of the respective sulfides, viz. -0.35–-0.38 e for Se compared to -0.47–-0.50 e for $ZnCr_2S_4$ and $CdCr_2S_4$ (28). The charges of $CoCr_2S_4$, $MnCr_2S_4$, and $FeCr_2S_4$ (1), however, resemble those of the selenides. This has been already deduced from the respective TO/LO splittings (18). The

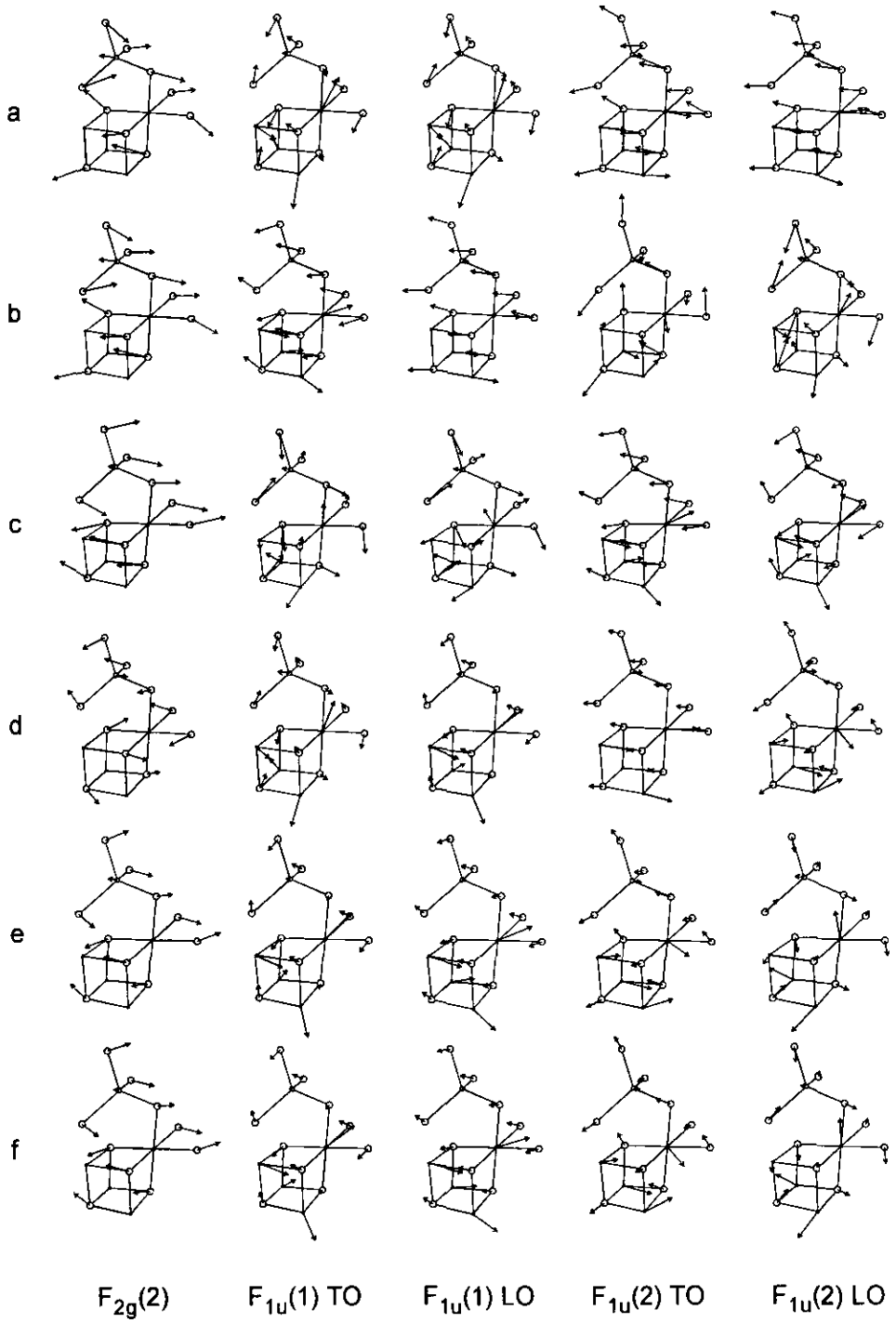

FIG. 3. Vibrational modes of the F_{2g} (2), F_{1u} (1) TO, F_{1u} (1) LO, F_{1u} (2) TO, and F_{1u} (2) LO phonons of $CoCr_2S_4$ (a), $ZnCr_2S_4$ (b), $CdCr_2S_4$ (c) (28), $ZnCr_2Se_4$ (d), $CdCr_2Se_4$ (e), and $HgCr_2Se_4$ (f).

positive charges mainly rest on the octahedrally coordinated Cr^{3+} ions. The charges of the tetrahedrally coordinated A^{2+} ions are nearly zero for both spinel-type sulfides and selenides.

As already shown by the experimental infrared and Raman spectra (5, 18) the eigenvectors (vibrational modes) and the potential energy distributions (PED) of the phonon modes of sulfide and selenide spinels differ more than expected for isostructural compounds with different masses of the atoms involved. The main differences worth mentioning concern (i) the vibrational modes of the Raman-allowed mode F_{2g} (1) and the transversal and

TABLE 4

Eigenvectors of the Raman-Allowed Phonon Modes of $CoCr_2S_4$, $ZnCr_2S_4$, $ZnCr_2Se_4$, $CdCr_2Se_4$, and $HgCr_2Se_4$ with Respect to the Symmetry Coordinate q (Ref. 1) Obtained by Polarizable-Ion Model Calculations

Compound	Species	q_1 (x)	q_2 (x)	q_3 (A)	q_4 (x)	q_5 (x)
$CoCr_2S_4$	A_{1g}	1.000				
	E_g		1.000			
	F_{2g} (1)					
	F_{2g} (2)			−0.086	−0.298	0.951
	F_{2g} (3)			−0.504	0.837	0.216
				0.860	0.460	0.222
$ZnCr_2S_4$	A_1	1.000				
	E_g		1.000			
	F_{2g} (1)			−0.144	−0.353	0.924
	F_{2g} (2)			−0.390	0.879	0.276
	F_{2g} (3)			0.910	0.320	0.264
$ZnCr_2Se_4$	A_{1g}	1.000				
	E_g		1.000			
	F_{2g} (1)			0.608	0.222	0.762
	F_{2g} (2)			−0.350	−0.787	0.508
	F_{2g} (3)			−0.713	0.575	0.401
$CdCr_2Se_4$	A_{1g}	1.000				0.849
	E_g		1.000			0.396
	F_{2g} (1)			−0.488	−0.204	
	F_{2g} (2)			0.330	0.857	
	F_{2g} (3)			0.808	−0.473	0.351
$HgCr_2Se_4$	A_{1g}	1.000				
	E_g		1.000			
	F_{2g} (1)			−0.381	−0.147	0.913
	F_{2g} (2)			0.352	0.890	0.290
	F_{2g} (3)			0.855	−0.432	0.287

Note. For the IR-allowed modes see Table 5, for the silent modes, see Ref. (28).

longitudinal optic phonons F_{1u} (1) and (2) (see Fig. 3) and (ii) the PEDs of A_{1g}, F_{2g} (1)–(3), F_{1u} TO (3) and (4), F_{1u} LO (3) and (4) (see Tables 6–8). In the case of the other modes, the differences are within the range of experimental and model errors.

Thus, in the case of the symmetry-restricted, total symmetric AX_4 breathing modes of species A_{1g}, the short-range force constants K_1, K_2, F_2, and F_3 are involved in different ways for the various spinel-type chromium chalcides. Whereas the influence of K_2 (CrX_6 octahedron) is nearly constant (25–32%, PIM), that of the A–X valence forces (K_1) increases in the order $MnCr_2S_4$ (1) = $FeCr_2S_4$ (1) < $CoCr_2S_4$ < $ZnCr_2S_4$ (27) < $CdCr_2S_4$ (28) < $ZnCr_2Se_4$ (27) < $CdCr_2Se_4$ < $HgCr_2Se_4$ from 15 to 41% and that of the X–X repulsive forces changes irregularly in the ranges 8–23% for F_2 and 12–35% for F_3. On the other hand, the likewise symmetry-restricted phonons of species E_g are dominated by the Cr–X (K_2) forces without significant variation among the spinel-type chromium chalcides (see Tables 6–8).

The PEDs of the symmetry-unrestricted phonons of species F_{2g} and F_{1u}, e.g., F_{2g} (1), F_{1u} (3) TO and LO, and F_{1u} (4) TO and LO, differ almost dramatically. Thus, in the case of F_{2g} (1) and F_{1u} (4) TO and LO, participation of K_1 ranges from <1% ($CoCr_2S_4$) to 73% ($ZnCr_2Se_4$) and from 3% ($ZnCr_2Se_4$) to 69% ($FeCr_2S_4$ (1)), respectively. The most intensive IR modes F_{1u} (1) and (2), both TO and LO, are dominated by K_2. The greatest participation of F_1 (long-range Cr–Cr interaction) was observed for F_{1u} (1) and (3). Long-range Coulomb forces (LRFC) mainly contribute to the E_g and F_{1u} (1) and (2) phonons.

DISCUSSION

The order of the A–X and Cr–X valence force constants of $CdCr_2Se_4$ and $HgCr_2Se_4$ is reversed, viz. 0.94 and 0.88, and 1.03 and 0.91 N cm^{-1} (PIM), respectively, compared to those of the corresponding sulfides, e.g., 0.89 and 1.00 N cm^{-1} for $CdCr_2S_4$ (28). The bond strengths of the A–X bonds increase in the order $ZnCr_2X_4$ < $CdCr_2X_4$ < Hg

TABLE 5

Eigenvectors of the IR-Allowed Phonon Modes of $CoCr_2S_4$, $ZnCr_2S_4$, $ZnCr_2Se_4$, $CdCr_2Se_4$, and $HgCr_2Se_4$ with Respect to the Symmetry Coordinates q (Ref. 1) Obtained by Polarizable-Ion Model Calculations

		q_6 (A)		q_7 (Cr)		q_8 (Cr)		q_9 (X)		q_{10} (X)	
Compound	Species	TO	LO	TO	LO	TO	LO	TO	LO	TO	LO
$CoCr_2S_4$	F_{1u} (1)	−0.063	−0.080	−0.159	−0.109	−0.264	−0.278	0.836	0.838	0.450	0.450
	F_{1u} (2)	0.162	−0.016	−0.652	−0.690	0.262	0.232	−0.351	−0.335	0.598	0.598
	F_{1u} (3)	0.837	0.835	0.044	−0.140	−0.537	−0.521	−0.098	−0.112	0.000	0.000
	F_{1u} (4)	−0.103	0.068	0.695	0.696	−0.057	−0.021	−0.251	−0.266	0.664	0.664
	F_{1u} (5)	0.509	0.540	0.255	0.093	0.755	0.773	0.326	0.320	0.000	0.000
$ZnCr_2S_4$	F_{1u} (1)	0.032	−0.109	−0.176	−0.136	0.543	0.545	0.673	0.673	0.469	0.469
	F_{1u} (2)	0.661	−0.694	−0.228	0.110	−0.319	−0.296	−0.246	−0.263	0.591	0.591
	F_{1u} (3)	0.311	−0.037	0.426	0.544	0.706	0.699	−0.473	−0.462	0.000	0.000
	F_{1u} (4)	−0.618	0.703	0.331	−0.002	−0.101	−0.123	−0.260	−0.244	0.657	0.657
	F_{1u} (5)	0.288	0.101	0.792	0.820	−0.309	−0.334	0.442	0.452	0.000	0.000
$ZnCr_2Se_4$	F_{1u} (1)	−0.204	−0.062	0.190	0.255	0.737	0.743	0.495	0.494	0.367	0.367
	F_{1u} (2)	0.042	0.556	0.806	0.604	−0.346	−0.314	−0.121	−0.114	0.463	0.463
	F_{1u} (3)	0.770	0.645	0.098	−0.424	0.470	0.478	−0.420	−0.419	0.000	0.000
	F_{1u} (4)	0.068	−0.291	−0.549	−0.463	−0.137	−0.158	−0.156	−0.159	0.807	0.807
	F_{1u} (5)	0.599	0.432	−0.055	−0.419	−0.313	−0.309	0.735	0.736	0.000	0.000
$CdCr_2Se_4$	F_{1u} (1)	−0.067	0.036	0.202	−0.195	−0.620	−0.624	−0.599	−0.600	0.460	0.460
	F_{1u} (2)	0.450	0.746	0.679	−0.351	0.333	0.303	0.173	0.182	0.442	0.442
	F_{1u} (3)	0.717	0.432	−0.310	0.655	−0.517	−0.514	0.350	0.347	0.000	0.000
	F_{1u} (4)	−0.218	−0.450	−0.510	0.318	0.179	0.198	0.258	0.254	0.770	0.770
	F_{1u} (5)	0.481	0.231	−0.376	0.556	0.453	0.464	−0.649	−0.650	0.000	0.000
$HgCr_2Se_4$	F_{1u} (1)	−0.034	0.035	0.161	−0.148	−0.543	−0.545	−0.595	0.597	0.569	0.569
	F_{1u} (2)	0.562	0.782	0.599	−0.276	0.335	0.304	0.215	−0.227	0.409	0.409
	F_{1u} (3)	0.637	0.351	−0.418	0.684	−0.545	−0.540	0.349	−0.343	0.000	0.000
	F_{1u} (4)	−0.296	−0.477	−0.471	0.277	0.241	0.260	0.351	−0.346	0.714	0.714
	F_{1u} (5)	0.436	0.189	−0.468	0.598	0.487	0.502	−0.595	0.596	0.000	0.000

Note. For the Raman-allowed modes see Table 4; for the silent modes see Ref. (28).

Cr_2X_4 as reflected by the increase in the force constants K_1 in the same direction (see Table 3). This behavior is obviously caused by the increase in strength of the covalent bonds from Zn to Hg compounds. In the same way, the larger K_1 of ACr_2S_4 (A = Zn, Cd), compared to those if A = Mn, Fe (1), and Co, are reasonable.

The most surprising results, however, are the findings that the A–X valence force constants of the spinel-type chromium selenides K_1 are equally large or even larger than those of the corresponding sulfides, e.g., 0.94 instead of 0.89 N cm^{-1} (28), but 0.88 and 1.00 N cm^{-1} (28) for K_2 in the case of the cadmium compounds. This is supported by the results of central force/angular force constant calculations, viz. α_1 = 0.68 and 0.57 N cm^{-1} and α_2 = 0.53 and 0.66 N cm^{-1}, respectively (6). The larger force constants of spinel-type chromium oxides compared to those of the sulfides, e.g., 1.80 and 0.87 N cm^{-1} for K_1 (PIM) of $ZnCr_2O_4$ (9) and $ZnCr_2S_4$ (27), respectively, are reasonable. They are supported by the O/S mass shifts of the respective A_{1g} and E_g modes, which display only X ion motions (see Ref. (1)), being greater than calculated, viz. 1.76–1.77 instead of 1.42. The respective S/Se mass shifts of these bands, however, are in the same range as observed, e.g., 1.62–1.69 for the A_{1g} modes of the Zn and Cd compounds (see Table 2) compared to 1.57 calculated from the respective masses, supporting the order of the force constants K_1 and K_2. The question arises whether the A–Se bonds in spinel-type chromium chalcides are stronger than the A–S bonds or whether other features are the reason for the findings discussed.

Apart from K_2 and F_1, the short-range force constants of the various spinel-type chromium chalcides do not depend greatly on the potential model chosen (see Table 3). This means, for example, in the case of the A–X force constant K_1 that bonding in the AX_4 tetrahedra is almost covalent as also revealed from the very low effective dynamical charges (<0.2 e) of the metal ions.

The increase in K_2 (Cr–X forces) on going from short-range model (SRM) to polarizable-ion model (PIM) calculations displays the change in the physical sense of this

TABLE 6

Potential Energy Distribution (PED %) of the Raman-Allowed Zone-Center Phonons of $CoCr_2S_4$, $CdCr_2Se_4$, and $HgCr_2Se_4$

Species	Force constant	$CoCr_2S_4$			$CdCr_2Se_4$		$HgCr_2Se_4$	
		SRM	RIM	PIM	SRM	PIM	SRM	PIM
A_{1g}	K_2	24	24	29	22	27	24	28
	K_1	18	18	19	37	37	40	41
	F_2	25	23	19	11	15	9	9
	F_3	24	23	27	21	16	24	18
E_g	K_2	67	71	88	76	88	80	92
	F_2	14	14	10	7	8		5
	F_3	14	13	15	13	9	14	10
	LRFC			−4		−8		−8
F_{2g} (1)	K_1				69	68	61	64
	K_2	31	32	37	18	22	24	27
	F_2	11	10	7	4	5		
	F_3	10	10	11	7	6	10	7
	F_4	33	31	35				
F_{2g} (2)	K_2	39	41	45	58	71	65	76
	K_1	37	36	39	6	7		
	F_4	14	14	11	18	11	20	11
F_{2g} (3)	K_2	24	26	32	51	57	48	55
	K_1	57	58	56	25	26	33	32
	F_2	6	6	5	6	7		4
	F_3	6	6	8	11	8	12	8

Note. LRFC, long-range Coulomb forces; for definition of the short-range force constants and further explanations, see Table 2. For values for $ZnCr_2S_4$ and $ZnCr_2Se_4$ see Ref. (27, 28).

TABLE 7

Potential Energy Distribution (PED %) of the IR-Allowed Zone-Center Phonons of $CoCr_2S_4$, $CdCr_2Se_4$, and $HgCr_2Se_4$

Species	Force constant	$CoCr_2S_4$					$CdCr_2Se_4$			$HgCr_2Se_4$		
			RIM		PIM			PIM			PIM	
		SRM	TO	LO	TO	LO	SRM	TO	LO	SRM	TO	LO
F_{1u} (1)	K_2	58	59	59	71	65	89	108	102	94	114	103
	K_1	5	5	5	3	5	2	3		2		
	LRFC				−19	−13		−20	−9		−20	−7
F_{1u} (2)	K_2	76	79	73	88	85	67	85	80	77	89	88
	K_1	10	10	8	14	7	22	19	18	17	19	16
	LRFC		−3	6	−11			−11	−8		−13	−10
F_{1u} (3)	K_1	24	23	25	25	28	65	67	70	67	68	70
	K_2	6	8	5	10	7	21	20	17	22	25	21
	F_1	32	29	30	32	30		5	5			
	F_2	14	13	13	11	11		2	2			
	F_3	13	13	13	15	16				6	4	4
F_{1u} (4)	F_2	10	9	9	9	8	21	28	28	21	25	24
	F_3	10	9	9	12	12	40	32	32	55	48	47
	K_1	60	62	62	58	60	12	13	13	14	14	13
	K_2		9	8	16	12						
	F_1	6		5	5	6		12	12		4	3
	H_2	6		5	3		27	14	14		12	12

Note. For explanations, see Tables 2 and 6. For $ZnCr_2S_4$ and $ZnCr_2Se_4$ see Ref. (27, 28).

TABLE 8
Potential Energy Distribution (PED %) of the Silent Zone-Center Phonons of $CoCr_2S_4$, $ZnCr_2S_4$, $CdCr_2S_4$, $ZnCr_2Se_4$, $CdCr_2Se_4$, and $HgCr_2Se_4$ (PIM)

Species	Force constant	$CoCr_2S_4$	$ZnCr_2S_4$	$CdCr_2S_4$	$ZnCr_2Se_4$	$CdCr_2Se_4$	$HgCr_2Se_4$
A_{2u} (1)	K_2	40	68	58	87	87	92
	F_1	55		22	4	9	
	K_1		25	11	6	6	8
	F_3		13	8			
	LRFC		−5	−9	−6	−7	−7
A_{2u} (2)	K_1	20	11	26	39	40	47
	F_1	19		43	11	10	
	F_2	19		7	27	16	11
	F_3	28	6	19	15	18	20
	K_2		35		10	5	14
	H_2		36				
E_u (1)	K_2	66	90	106	109	111	113
	LRFC	−7	−10	−29	−17	−20	−18
	F_4	26	13	9		3	
E_u (2)	F_4	27	14	19	54	24	36
	F_2			5	18	15	14
	F_3			13	15	17	26
	F_1	50		98	16	15	4
	H_2	12	73			43	
	K_2	10	29	43	29		
	LRFC	−7	−22	−77	−48	−22	−39
F_{1g}	K_2	75	89	109	103	105	106
	F_4	27	11	8	9	5	5
	LRFC		−8	−16	−13	−13	−13
F_{2u} (1)	K_2	85	99	136	122	119	120
	H_2		10			4	
	F_4	22	7	7			
	LRFC	−10	−17	−43	−24	−24	−23
F_{2u} (2)	F_4	63	28	157	148	50	68
	LRFC	−16	−10	−310	−93	−25	−36
	K_2	31	10	253	44	10	16
	H_2	22	72			65	52

Note. For explanations see Tables 2 and 6.

force constant connected with these models, namely Pauli-type electronic repulsion for PIM, but both Coulomb and repulsive forces in the case of SRM. The differences between the respective figures, e.g., 0.16 N cm^{-1} for $CoCr_2S_4$, vary with the effective charges of the chromium ions, viz. $CdCr_2S_4 > ZnCr_2S_4 > CoCr_2S_4 = CdCr_2Se_4 > ZnCr_2Se_4 \sim HgCr_2Se_4$ (see Table 3) and, hence, are a measure of the ionicities of the compounds under discussion.

The values obtained for F_1 (Cr–Cr interaction) are likewise somewhat increased in the PIM calculations (with the exception of $ZnCr_2S_4$, which may be due to calculation errors) (see Table 3 and Ref. 1). From these findings, attractive bonding forces between the d orbitals of the d^3 Cr^{3+} ions may be concluded. In the case of $ZnCr_2O_4$ (9), F_1 is strongly decreased in the PIM calculations compared to that of SRM, possibly revealing antibonding d–d interactions.

The differences in the vibrational modes (and potential energy distributions) of some phonon modes within the isostructural series under discussion, so far as they are not due to the different masses of the atoms involved, are obviously caused by the different ionicities; hence the importance of Coulomb forces for the lattice potential. Therefore, particularly the vibrational modes of phonons, which are dominated by such forces (LRFC), as F_{1u} (1)

and F_{1u} (2), differ strongly (see Fig. 3). In the case of aspects not discussed in this paper, the results and conclusions given in Ref. (1, 9, 27) have been confirmed.

CONCLUSION

High-level lattice dynamical calculations are a powerful technique for studying both the strength of individual bonds in solids and the nature of the phonon modes. Thus, in the case of spinel-type chromium chalcides, these calculations elucidate the different bondings of the tetrahedrally and octahedrally coordinated metal ions and establish the trends of the bond strengths and ionicities within this class of compounds. The character of the various phonons as relating to eigenvectors and potential energy distributions differs to a much larger extent than expected for isostructural compounds. Therefore, discussions of frequency shifts observed in ordinary IR and Raman spectra with respect to bonding features must be taken with caution.

REFERENCES

1. H. D. Lutz, J. Himmrich, and H. Haeuseler, *Z. Naturforsch. A* **45,** 893 (1990).
2. P. Bruesch and F. D'Ambrogio, *Phys. Status Solidi B* **50,** 513 (1972).
3. H. D. Lutz and H. Haeuseler, *Ber. Bunsenges. Phys. Chem.* **79,** 604 (1975).
4. K. Wakamura, H. Iwatani, and K. Takarabe, *J. Phys. Chem. Solids* **48,** 857 (1987).
5. H. D. Lutz, W. Becker, B. Müller, and M. Jung, *J. Raman Spectrosc.* **20,** 99 (1989).
6. H. C. Gupta, M. M. A. Parashar, V. B. Gupta, and B. B. Tripathi, *Physica B (Amsterdam)* **167,** 175 (1990).
7. H. C. Gupta, M. M. Sinha, K. B. Chand, and Balram, *Phys. Status Solidi B* **169,** K65 (1992).
8. H. C. Gupta, M. M. Sinha, K. B. Chand, and Balram, *J. Phys. Chem. Solids* **53,** 775 (1992).
9. J. Himmrich and H. D. Lutz, *Solid State Commun.* **79,** 447 (1991).
10. J. Zwinscher, H. C. Gupta, and H. D. Lutz, *J. Phys. Chem. Solids* **55,** 287 (1994).
11. H. A. Lauwers and M. A. Herman, *J. Phys. Chem. Solids* **41,** 223 (1980).
12. E. F. Steigmeier and G. Harbeke, *Phys. Kondens. Mater.* **12,** 1 (1970).
13. K. Wakamura, T. Arai, and K. Kudo, *J. Phys. Soc. Jpn.* **40,** 1118 (1976).
14. N. Koshizuka, Y. Yokoyama, and T. Tsushima, *Solid State Commun.* **23,** 967 (1977).
15. M. Iliev, G. Güntherodt, and H. Pink, *Solid State Commun.* **27,** 863 (1978).
16. M. Iliev, E. Anastassakis, and T. Arai, *Phys. Status Solidi B* **86,** 717 (1978).
17. K. Wakamura, T. Ogawa, and T. Arai, *Jpn. J. Appl. Phys.* **19**(Suppl. 19-3), 249 (1980).
18. H. D. Lutz, G. Wäschenbach, G. Kliche, and H. Haeuseler, *J. Solid State Chem.* **48,** 196 (1983).
19. K. Beckenkamp, private communication.
20. H. D. Lutz, W. W. Bertram, B. Oft, and H. Haeuseler, *J. Solid State Chem.* **46,** 56 (1983).
21. H. V. Philipsborn and H. Treitinger, *in* "Landolt-Börnstein Zahlenwerte und Funktionen aus Physik" Neue Folge, Vol. III 12b, p. 300. Springer-Verlag, Berlin, 1980.
22. M. Robbins, P. Gibart, D. W. Johnson, R. C. Sherwood, and V. G. Lambrecht, *J. Solid State Chem.* **9,** 170 (1974).
23. H. D. Lutz, W. Becker, and W. W. Bertram, *J. Solid State Chem.* **37,** 165 (1981).
24. H. Rej, A. Bombik, J. Kusz, A. Oles, M. Pinod, and J. Warczewski, *Mater. Sci. Forum* **79–82,** 771 (1991).
25. T. N. Borovskaya, L. A. Butman, V. G. Tsirel'son, M. A. Porai-Koshits, T. G. Aminov, and R. P. Ozerov, *Kristallografiya* **36,** 612 (1991).
26. D. Konopka, A. Slebarski, and A. Chelkowski, *Acta Phys. Pol. A* **46,** 47 (1974).
27. J. Zwinscher and H. D. Lutz, *J. Alloy Comp.* **219,** 103 (1995).
28. J. Zwinscher, Ph.D. Thesis, University of Siegen, 1995.